Determinants of Left Ventricular Shape Change During Filling

Jeffrey W. Holmes
M.D., Ph.D.
Department of Biomedical Engineering,
Columbia University,
New York, NY 10027

Left ventricular shape and shape change are easy to measure and their analysis has been proposed as a noninvasive method to determine myocardial anisotropy. In preparation for applying this approach to studies of rats with experimentally induced cardiac hypertrophy, the goals of this study were to describe normal shape changes during diastolic filling in the rat and to utilize a finite-element model to estimate the relative importance of three factors that determine left ventricular shape change during filling: global chamber compliance, fiber to crossfiber stiffness ratio, and fiber architecture. The results suggest that left ventricular shape change is least sensitive to fiber to cross fiber stiffness ratio, and that this will likely limit the practical utility of using shape changes to diagnose changes in myocardial anisotropy. [DOI: 10.1115/1.1645527]

Introduction

Left ventricular shape and shape change have been studied extensively in large animals and in patients [1–5]. Because ventricular shape is easy to measure noninvasively and is known not only to change in some disease states but also to predict clinical prognosis [6], the ability to relate ventricular shape or shape changes to underlying myocardial mechanics could be of diagnostic value. For example, it was recently proposed that the ratio of fiber to cross fiber stiffness of the myocardium can be deduced in patients from the pattern of volume and shape changes during left ventricular filling [7].

In a series of studies thirty years ago, Rankin and coworkers studied dimension and shape changes in the canine left ventricle [1–3]. They found remarkably linear relationships between eccentricity (a measure of shape) and ventricular volume during both diastolic filling and systolic ejection. During filling, the ventricle becomes more spherical; during ejection, it becomes more elliptical [2,3]. In addition, they found that the slope of the shape/volume curve is much steeper during filling than during ejection [2,3].

Sphericalization of the left ventricle during filling would be predicted from a simple analysis of the underlying mechanics. At the equator of an ellipsoidal shell, circumferential wall stresses are greater at a given cavity pressure than longitudinal stresses. If the shell is composed of an isotropic material, more stretch will be induced in the circumferential than in the longitudinal direction at each cavity pressure, resulting in sphericalization during inflation [8]. If the shell is composed of an anisotropic material, increasing circumferential to longitudinal stiffness ratios will reduce and eventually reverse the slope of the shape/volume relationship during inflation.

Extending this reasoning to the left ventricle, we hypothesized that the following factors would influence the extent of shape change during filling. First, a ''stiffer'' ventricle will clearly experience less volume and shape change during inflation to a given pressure; global chamber compliance, which depends on both chamber geometry and material properties, should therefore be one determinant of ventricular shape change. Second, passive myocardium is stiffer along the local fiber direction than transverse to it [9–11], so both the fiber to crossfiber stiffness ratio and the transmural distribution of fiber orientations should determine the effective circumferential to longitudinal stiffness ratio of the ventricle and thereby influence the extent of shape change during filling.

This study therefore had two goals with respect to understanding ventricular shape/volume relationships and their potential utility in the study of cardiac disease. The purpose of the experimental studies was to describe normal shape changes during diastolic filling in the rat as a basis for comparison for studies in rats with experimentally induced cardiac disease. The purpose of the model studies was to estimate the relative importance of three factors expected to determine the extent of left ventricular shape change during filling: 1) global chamber compliance, 2) fiber to crossfiber stiffness ratio, and 3) fiber architecture.

Methods

Experimental Data Collection. We previously reported hemodynamic changes during early volume overload in adult male Sprague-Dawley rats [12]. Sonomicrometry data from the seven-day sham animals in that study ($n=8$) were re-analyzed for the present study to calculate left ventricular shape, not considered in the original report. All studies were performed in accordance with the Guide for Care and Use of Laboratory Animals [13] and approved by Columbia University's Institutional Animal Care and Use Committee. Sham animals underwent an abdominal surgery to expose and temporarily (<5 minutes) occlude the abdominal aorta and vena cava. The abdomen was closed, postoperative analgesia administered, and the animals allowed to recover.

One week after sham surgery, animals were anesthetized with isoflurane (3.5% induction, 2.5–3.0% maintenance) and ventilated at 60 breaths per minute with a tidal volume of approximately 3.0 ml. Body temperature was maintained with a warming pad. The chest was opened by midline sternotomy, bleeding was controlled by electrocautery and a retractor was placed. Four 1.0-mm sonomicrometers (Sonometrics, Ontario, Canada) were sewn to the epicardium with 6-0 silk suture on the posterior wall 2/3 of the distance from apex to base, just lateral to the interventricular groove (posterior); on the anterior wall 2/3 of the distance from apex to base and just lateral to the interventricular groove (anterior); on the lateral freewall under the atrial appendage (base); and at the left ventricular apex (apex). A calibrated Millar SP-671 miniature pressure transducer (Millar Instruments, Houston, TX) was inserted into the left ventricle through the anterior wall, the retractor removed and hemostasis verified. Instrumentation required 40–45 minutes from induction of anesthesia. Five seconds of segment length and pressure data were acquired at 312 Hz every 5 minutes for the subsequent hour using the Sonometrics software SonoLab. Following data acquisition, the animals were

Corresponding address: Biomedical Engineering ET 351, Columbia University MC 8904, 1210 Amsterdam Avenue, New York, NY 10027. Phone: (212) 854-6530; Fax: (212) 854-8725; e-mail: jh553@columbia.edu.

Contributed by the Bioengineering Division for publication in the JOURNAL OF BIOMECHANICAL ENGINEERING. Manuscript received by the Bioengineering Division June 19, 2003; revision received October 9, 2003. Associate Editor: J. Humphrey.

heparinized and the hearts arrested and rapidly removed. The position of the sonomicrometers was recorded and the left ventricular weight determined.

Experimental Data Analysis. Sonomicrometer signals required minimal filtering or correction. The best quality anterior-posterior and apex-base signals were selected for each animal and exported along with ventricular pressure to ASCII files for analysis using a custom routine written in Matlab (v. 5.0, The MathWorks, Natick, MA). Premature ventricular contractions and one subsequent beat were excluded from analysis. The ventricle was treated as a prolate spheroid truncated 50% of the distance from equator to base as suggested by Streeter and Hanna [14]. Left ventricular cavity plus wall volume was calculated from the epicardial anterior-posterior (AP) and base-apex (BA) lengths according to their Equation (20) with $f_b=0.5$ (Equation (1)); cavity volume was determined by subtracting wall volume calculated as the measured left ventricular weight divided by a density of 1.06 g/cm^3.

$$V=\frac{\pi}{3}(2+3(0.5)-(0.5)^3)\left(\frac{AP}{2}\right)^2\left(\frac{BA}{1.5}\right)=1.125\frac{\pi}{6}AP^2BA \tag{1}$$

Mean wall thickness (h) was calculated at each cavity volume assuming that wall volume remained constant throughout the cardiac cycle. Endocardial minor (SA) and major (LA) radii were then calculated according to Equation (2) and shape (S) was defined as their ratio:

$$SA=\frac{AP}{2}-h;\quad LA=\frac{BA}{1.5}-h;\quad S=\frac{SA}{LA} \tag{2}$$

For comparison to results from Rankin's group in dogs, eccentricity (E) was calculated from epicardial segment lengths and mean wall thickness according to their definition [1]:

$$E=\left(\frac{(BA-0.55h)^2-(AP-h)^2}{(BA-0.55h)^2}\right)^{0.5} \tag{3}$$

Heart rate averaged 385 beats per minute, slightly more than 6 Hz, in the eight animals studied. Each 5-second data run recorded at 312 Hz therefore included roughly 30 beats, each represented by approximately 50 points. All data from each beat were interpolated at 50 evenly spaced time points and averaged to generate mean interpolated curves representing each 5-second data run. Stability of the preparation was verified by confirming $\leqslant$5% variation in each parameter between the runs at 15, 30, and 45 minutes; the interpolated curves from these time points were then averaged. Finally, these interpolated curves from each of the eight animals were averaged. Phases of the cardiac cycle were identified as follows: end diastole was selected as the time point immediately preceding the rapid pressure upstroke, the beginning of ejection as the end of the rapid pressure upstroke, end systole as the point of maximal elastance (LVV/LVP), and the beginning of filling as the time of minimum left-ventricular pressure (Fig. 1).

Finite-Element Model. The finite-element model used for this study was similar to that originally reported by Costa et al. [15] and used by Emery et al. in recent studies of rat ventricular mechanics [16,17]. The left ventricle was modeled as an axisymmetric thick-walled ellipsoid using three bicubic-linear prolate spheroidal finite elements. Endocardial short- and long-axis dimensions and uniform wall thickness were matched to average experimental dimensions at the onset of filling by appropriate choice of focal length and nodal coordinate values. Fiber angles varied linearly from the epicardium to the endocardium with specific values depending on the simulation (see below). The boundary conditions for this study were slightly different from those used by Emery [16,17]. When simulating passive inflation of the rat left ventricle, their model extended 30 deg above the equator and displacement was prevented at the basal nodes to simulate

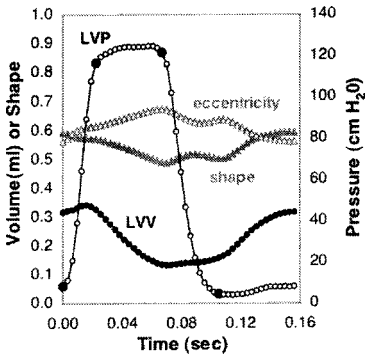

Fig. 1 Mean left ventricular pressure (LVP, open circles), volume (LVV, solid circles), shape (solid triangles), and eccentricity (open triangles) curves in eight sham-operated control rats. Large solid circles on pressure tracing indicate (from left) end diastole, beginning of ejection, end of ejection, and beginning of filling.

attachment to a rigid cannula at the mitral valve orifice. Because we were simulating in vivo shape changes and did not want our boundary conditions to artificially constrain short-axis displacement, we modeled the lower 2/3 of the left ventricle, truncating the mesh at the equator and imposing symmetry boundary conditions at the equatorial nodes: no longitudinal displacement, no change in angle between the endocardial and epicardial surfaces and the basal plane, and no constraints on radial displacement. The model was implemented in Continuity, a finite-element software package developed and made available by the Cardiac Mechanics Research Group at the University of California, San Diego (http://cmrg.ucsd.edu).

The stress-strain behavior of passive myocardium was modeled using a hyperelastic strain-energy function in terms of strains expressed relative to the local fiber (f), cross fiber (c), and radial (r) directions [18,19]:

$$W=\frac{1}{2}C(e^Q-1)\quad\text{where}$$
$$Q=b_1E_{ff}^2+b_2(E_{cc}^2+E_{rr}^2+2E_{cr}^2)+b_3(2E_{fr}^2+2E_{fc}^2) \tag{4}$$

Material parameters were not formally optimized. Using previous studies by Omens and co-workers [18,19] as a guide, values of $C=0.5$, $b_1=b_2=b_3=4$ were selected as a starting point for the isotropic simulations and found to provide a reasonable match to experimental pressure-volume behavior. Material constants were then varied as described below for each series of simulations.

Model Simulations. Three sets of model simulations were performed. In each case, the model was inflated passively from 0 to 1.0 kPa (10.2 cmH_2O) in 10 steps and the deformed geometry recorded for each step. In the first set, an isotropic material was simulated by setting all exponential material constants equal ($b_1=b_2=b_3$) and varying the value of those constants from 2.5 to 10. In the second set of simulations, a transversely isotropic material was simulated by setting $b_2=b_3=4$ and varying the value of b_1, the constant controlling fiber stiffness. To maintain approximately constant global chamber compliance, C was gradually decreased as b_1 was increased; to achieve the highest b_1/b_2 ratios, the values of b_2 and b_3 were also decreased. For this simulation, fiber orientations varied linearly from -52 deg (clockwise from circumferential) on the epicardium to $+53$ deg on the endocardium, the distribution used by Omens et al. [18,19] and Emery et al. [16,17] in their models of the rat left ventricle based on their fiber angle measurements. In the third set of simulations, fiber stiffness was again varied but the transmural distribution was shifted by 10 deg, to -42 deg on the epicardium and $+63$ deg on the endocardium.

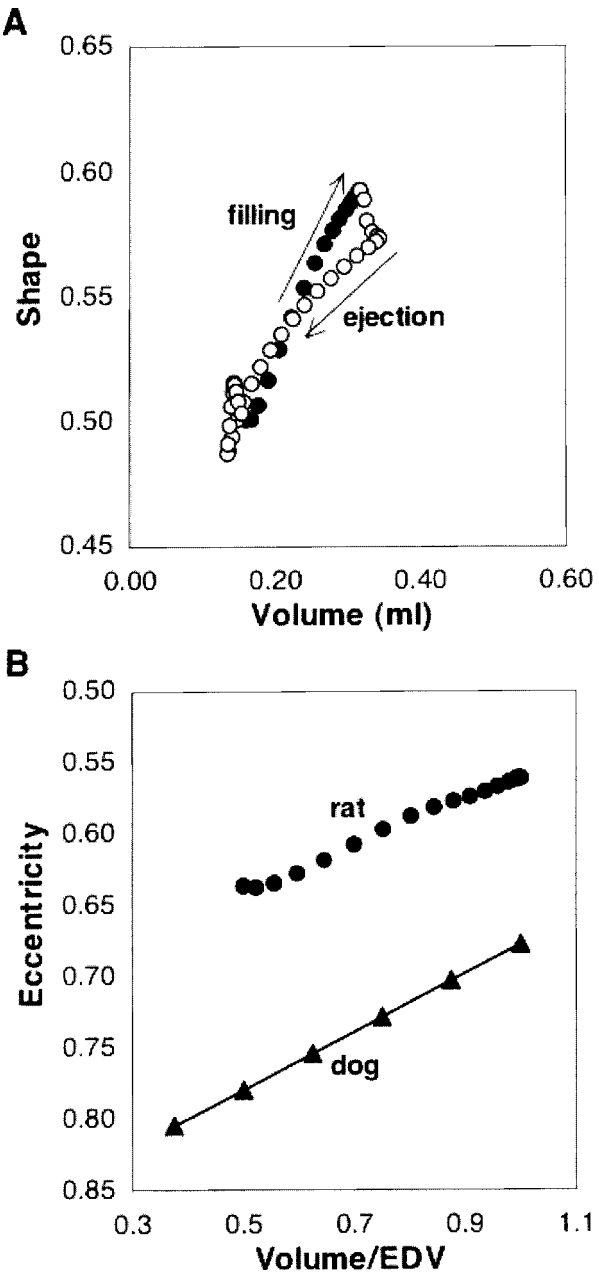

Fig. 2 Left ventricular shape/volume relationships. (*a*) Mean data from eight rats demonstrate sphericalization (increasing shape) of the left ventricle during filling (solid circles) and ellipticalization during ejection. (*b*) Plotting eccentricity, a different measure of shape, against normalized volume for comparison with canine data from Rankin 1980 [2] reveals that behavior of rat (circles) and dog (triangles) ventricles is similar, with the rat LV more spherical at all volumes.

Results

Left Ventricular Shape Changes in the Rat. Average left ventricular volume, pressure, shape, and eccentricity curves for 8 animals studied one week after sham operation are shown in Fig. 1. As expected, the rat left ventricle becomes more elliptical during ejection and more spherical during filling. Eccentricity and shape changes were opposite in sign as expected from their definitions and of equal magnitude (Fig. 1). Since these indices provide similar information, the remainder of the study focused on the simpler shape index as defined in Equation (2).

Plotting shape against volume produced loops similar to those reported by Rankin's group in dogs (Fig. 2*a*) [2,3]. Shape and volume were linearly related during filling (R^2 0.977$\pm$0.020, linear fit RMS error 0.004$\pm$0.003) and ejection (R^2 0.960$\pm$0.038, RMS error 0.006$\pm$0.008), with a steeper slope during filling ($P=0.007$, paired *t*-test). When normalized by end-diastolic volume, Rankin's canine filling data and our rat filling data produced eccentricity vs. volume curves with similar slopes but different intercepts; the rat left ventricle was more spherical than the dog left ventricle throughout the volume range studied (Fig. 2*b*).

Calculated slopes of the shape/volume relationships varied widely (Table 1). While the 95% confidence interval was only $\pm$28% of the mean value (0.317$\pm$0.090 ml) for end-diastolic volume and $\pm$10% of the mean for end-diastolic shape (0.592 $\pm$0.058), the 95% confidence interval for the slope of the shape/volume filling relationship was $\pm$50% of the mean (0.626 $\pm$0.312 ml^{-1}). For ejection the 95% confidence interval was $\pm$62% of the mean (0.451$\pm$0.279 ml^{-1}). We considered possible approaches to normalizing for variation in ventricular size or shape. End-diastolic volume and wall thickness, but not shape, were significantly correlated with the slope of the shape/volume relationship; ventricles with smaller end-diastolic volumes and larger wall thicknesses had steeper slopes. Normalizing by wall thickness had little effect on the variability of the calculated slopes, but normalizing cavity volume by end-diastolic volume greatly reduced the relative confidence intervals, to $\pm$20% of the mean slope for filling and $\pm$39% for ejection (Table 1).

Effect of Global Chamber Compliance. The influence of global chamber compliance on shape change was tested by simulating passive inflation to 1.0 kPa of a model ventricle composed of an isotropic material with a varying exponential material constant ($b_1=b_2=b_3$ in Equation 4). In the material constant range 3 to 6, global chamber compliance as reflected in the slope of the pressure-volume curve was similar to the average experimental results (Fig. 3*a*). The simulations traced out different portions of a single nonlinear shape/volume curve and covered a range of volume and shape changes similar to the experimental values (Fig. 3*b*). We calculated the ratio of total shape change to total volume change ($\Delta S/\Delta V$) for each simulation and found that a two-fold variation in the material constant produced values that covered the central half of the experimental 95% confidence interval (Fig. 3*c*). However, after normalizing by end-diastolic chamber volume, material stiffness had little effect on the shape/volume relationship; the same two-fold variation in the material constant produced only a 9% change in $\Delta S/(\Delta V/EDV)$, and a four-fold variation produced only a 15% change (Fig. 3*c*).

Effect of Fiber Stiffness and Orientation. The influence of fiber to crossfiber stiffness ratio was tested in two series of simulations. First, using the fiber distribution employed by Omens and coworkers in similar models based on their measurements in rats (linear variation from -52 deg at the epicardium to $+53$ deg at the endocardium) [16–19], the material constant governing fiber stiffness (b_1 in Equation 4) was increased while the scaling constant in the material law (C) was decreased to hold overall chamber compliance approximately constant (Fig. 4*a*). Normalized $\Delta S/\Delta V$ was calculated for inflation to 1.0 kPa for each set of material constants. Increasing fiber stiffness reduced shape change and $\Delta S/\Delta V$ (Fig. 4*b*). By varying the ratio of the fiber to crossfiber material constants from 1 to 4, it was possible to cover the entire 95% confidence interval of the experimental normalized $\Delta S/\Delta V$ values (Fig. 4*c*, open circles). If the fibers were made stiff enough, sphericalization of the model during simulated filling could be completely prevented; this occurred at a fiber to crossfiber material constant ratio of between 30 and 40 (Fig. 4*c*).

Next, the entire series of simulations was repeated with a slightly shifted transmural fiber distribution (-42 to $+63$ deg); this 10 deg shift was within the measurement uncertainty in reported measurements of myocardial fiber angle [20,21]. With the shifted

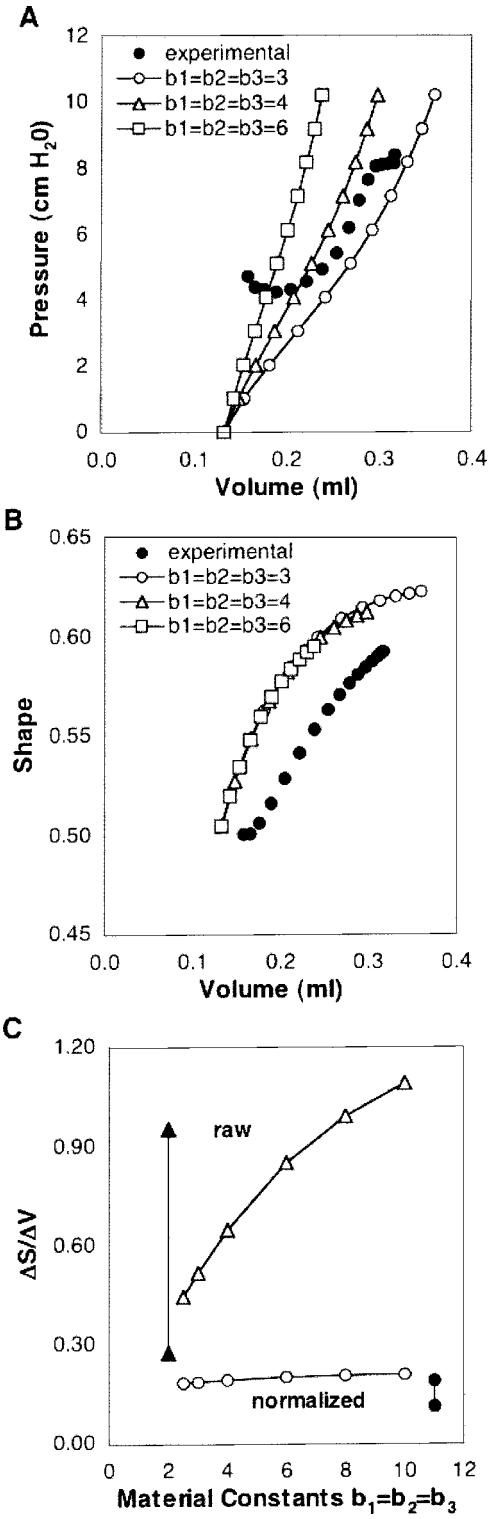

Fig. 3 Model simulations of the effect of global chamber compliance on shape change. (*a*) Mean experimental (closed symbols) and model pressure-volume behavior (open symbols) at 3 different values of the isotropic exponential material constant $b_1=b_2=b_3$ ($C=0.5$ for all simulations). (*b*) Corresponding mean experimental and model shape/volume curves. (*c*) Model behavior across a larger range of material constants. A threefold change in the material constant produced shape change/volume change ratios ($\Delta S/\Delta V$, open triangles) that covered a range similar to the 95% confidence interval of the experimental data (closed triangles), while normalized ratios ($\Delta S/(\Delta V/EDV)$, open circles) remained constant and slightly outside the experimental range (closed circles) for all simulations.

distribution, a range of fiber to crossfiber material constant ratios from 1 to 15 was required to cover the 95% confidence interval of the experimental data (Fig. 4*c*, open triangles).

Discussion

The goals of this study were to describe normal ventricular shape changes during filling in the rat and to use a finite-element model of the passive left ventricle to estimate the relative importance of three factors to those shape changes: 1) global chamber compliance, 2) fiber to cross fiber stiffness ratio, and 3) fiber architecture. Specifically, we were intrigued by the possibility that ventricular shape changes might offer a convenient way to assess myocardial fiber to crossfiber stiffness ratios in animals and patients using information that can be obtained noninvasively in the intact ventricle [7]. The experimental data presented here demonstrate that rats have similar linear shape/volume filling curves to those described previously in dogs. The modeling results suggest that shape change during filling is more sensitive to both global chamber compliance and to the transmural distribution of fiber orientations than to myocardial anisotropy. While the effect of global chamber compliance can be easily accounted for by normalizing by end-diastolic volume, it appears that very precise knowledge of fiber angle distribution would be needed to draw useful conclusions about changes in myocardial anisotropy from left ventricular shape changes.

Normalization of Shape/Volume Data. We initially discovered that normalizing volume data by end-diastolic volume reduces variability in shape change to volume change slopes and ratios ($\Delta S/\Delta V$) by trial and error; we tested factors that correlated with slope and found that normalizing by end-diastolic volume produced the greatest reduction in the size of the 95% confidence interval relative to the mean. However, the modeling studies provide a more convincing rationale for this normalization. In situations where end-diastolic pressures are about the same across the animals or patients studied (as in this study), individual end-diastolic volumes include information both about the overall size of the left ventricle and about its global compliance. Thus, normalizing by end-diastolic volume accounts for one of the three factors that influence shape change, making it easier to extract information about the others. It should be noted that when making comparisons among animals or patients with very different filling pressures, this normalization may not be as effective, since end-diastolic volume will also incorporate information about filling pressures.

Sensitivity to Fiber Architecture. The most surprising finding of this study is the very high sensitivity of model shape change to small changes in the transmural distribution of fiber orientations. This raises real concerns about the practicality of using patient or even animal data to diagnose individual fiber to cross fiber stiffness ratios. Experimental measurements suggest that fiber angles vary considerably from animal to animal and even spatially within a single heart [20–23]. MacKenna et al. reported epicardial fiber angles of -56 ± 12 deg (SEM, $n=8$) and endocardial fiber angles of 45 ± 23 deg with linear variation across the wall [21]. That group's finite-element models of the rat heart have typically employed a symmetric, linear transmural distribution from -52 to 53 deg, and we used the same distribution for our first series of simulations on the impact of material anisotropy (Fig. 4*c*, open circles). However, their measurements translate to 95% confidence intervals of ±24 deg on the epicardium and ±45 deg on the endocardium, confirming that the 10 deg shift applied in our second series of simulations (Fig. 4*c*, open triangles) was well within typical measurement uncertainty. Streeter and Hanna found that epicardial and endocardial fiber angles changed by roughly 10 deg from base to apex in the dog, and that endocardial fiber angles changed by a similar amount between diastole and systole [20], suggesting that using models with regionally uniform

Table 1 Shape data during filling in 8 sham-operated rats. EDV=end diastolic volume; EDS=end diastolic shape; $\Delta S/\Delta V$ =change in shape during filling divided by change in cavity volume; slope, int, R^2 and RMS err=slope, intercept, squared correlation coefficient and RMS error of linear fit to shape vs. volume data for each animal; $\Delta S/\Delta V_n$=normalized ratio ($\Delta S/(\Delta V/EDV)$); $slope_n$=normalized shape/volume slope (slope*EDV); CI=confidence interval.

	EDV	EDS	$\frac{\Delta S}{\Delta V}$	slope	int	R^2	RMS err	$\frac{\Delta S}{\Delta V_n}$	$slope_n$
AVF 039	0.192	0.506	1.105	1.028	0.315	0.979	0.008	0.212	0.197
AVF 046	0.357	0.535	0.460	0.492	0.361	0.997	0.001	0.164	0.175
AVF 055	0.309	0.515	0.401	0.468	0.373	0.988	0.004	0.124	0.144
AVF 060	0.160	0.631	1.622	1.577	0.386	0.982	0.011	0.259	0.252
AVF 064	0.272	0.619	0.425	0.400	0.513	0.929	0.002	0.116	0.109
AVF 068	0.319	0.599	0.318	0.384	0.479	0.976	0.003	0.101	0.123
AVF 076	0.338	0.764	0.378	0.438	0.617	0.981	0.004	0.128	0.148
AVF 083	0.588	0.569	0.200	0.222	0.437	0.979	0.002	0.117	0.130
Mean	0.317	0.592	0.614	0.626	0.435	0.977	0.004	0.153	0.160
SD	0.130	0.084	0.489	0.450	0.098	0.020	0.003	0.056	0.047
95% CI	±0.090	±0.058	±0.339	±0.312	±0.068	±0.014	±0.002	±0.039	±0.032
CI/mean	±0.28	±0.10	±0.55	±0.50	±0.16			±0.25	±0.20

fiber distributions may also prevent confident conclusions about material anisotropy even if the fiber distributions are measured with unusual accuracy for each individual analyzed.

Experimental Limitations and Sources of Error. The Sonometrics dimension measurement system has excellent spatial (μm) and temporal resolution (ns) more than adequate for the studies performed here. The largest source of error in the calculated volumes and shapes was the assumption of a spatially uniform wall thickness calculated from the measured wall volume. We did not attempt to measure wall thickness or endocardial dimensions directly because of evidence that sonomicrometer placement into the myocardial wall impairs function [24]. Because wall thickness was likely actually somewhat smaller at the apex than at the equator, this error may have resulted in calculated shape ratios that were larger (more spherical) than the actual ventricle. At the mean end-diastolic epicardial dimensions in this study, if apical thickness were in fact one half of equatorial thickness, our approach would result in a 20% overestimation of S and ΔS.

Another limitation is that volume and shape changes were measured in the open-chest, anesthetized state in sham-operated animals. Rankin and coworkers found that the open-chest, anesthetized state moved animals to lower volumes on their shape/volume curves but did not change the curves themselves [1–3], suggesting that this limitation of our analysis is unlikely to fundamentally change the findings. Because the sham operation did not require entering the chest, animals regained a normal body weight growth curve on postoperative day 2 (5 days before they were studied), and our calculated cardiac output values in these sham-operated animals were very similar to those reported by a number of investigators in both open- and closed-chest normal and sham-operated rats using a variety of other techniques (radioactive microspheres, thermodilution, etc.) [12], we concluded that these sham-operated rats fairly represent ''normal'' ventricular hemodynamics and could not justify the sacrifice of new unoperated control animals for the present study.

Limitations of the Model Analysis. This study employed a validated, well-established and tested finite element model featuring finite elasticity, a realistic geometry, material anisotropy and a transmurally varying distribution of fiber orientations. However, a number of other features of ventricular mechanics that might influence shape were not included. Neither the papillary muscles nor the attachments to the valve rings and great vessels were represented in the model [25]. The laminar structure of the myocardium was not incorporated [26]. Although residual stresses are known to exist in the unloaded intact rat ventricle [27], residual stress was not included in the finite-element model used for these studies. Because the shape behavior of the model was quite similar to our experimental measurements even without formal material parameter optimization, it seems unlikely that any of these factors represents such a large omission as to invalidate the entire analysis. The omission of residual stress is probably the most important; a typical residual stress pattern would decrease endocardial stresses and therefore the contribution of endocardial fibers to shape behavior, while increasing epicardial stresses and the contribution of epicardial fibers to shape behavior. For symmetric fiber distributions this should have little effect on shape behavior. However, since longitudinally oriented endocardial fibers promoted sphericalization in the particular nonsymmetric distribution tested in this study (Fig. 4), the inclusion of residual stress might have reduced the difference in shape behavior between this distribution and the symmetric distribution used for comparison.

Conclusions

In summary, the experimental data presented here demonstrate that rats have similar linear shape/volume filling curves to those described previously in dogs. The modeling results suggest that shape change during filling is more sensitive to both global chamber compliance and to the transmural distribution of fiber orientations than to myocardial anisotropy. We conclude that very precise knowledge of fiber angle distributions would be needed to draw useful conclusions about changes in myocardial anisotropy from left ventricular shape changes and that this requirement will likely limit the practical utility of this approach.

Acknowledgments

The author wishes to acknowledge the Whitaker Foundation (RG-00-0062) and National Science Foundation (BES-02-0167) for financial support of this project, Dr. Andrew McCulloch at the University of California San Diego for providing the finite element software Continuity through the National Biomedical Computation Resource (NIH P41RR08605), and Drs. Jeffrey Omens and Kevin Costa for discussion and suggestions.

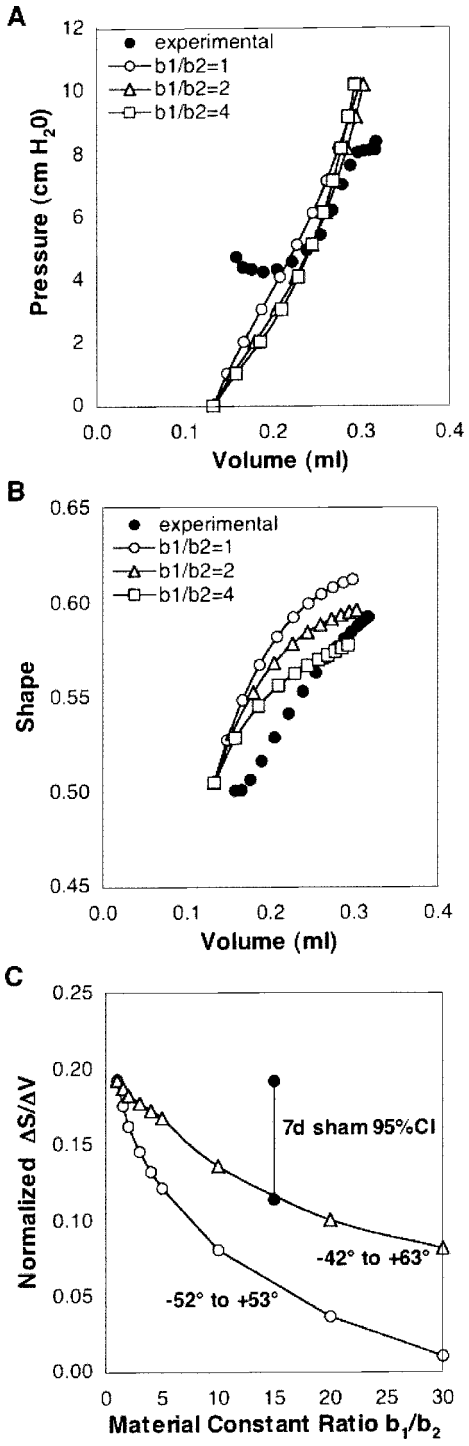

Fig. 4 Model simulations of the effect of fiber stiffness and orientations on shape change. (*a*) Mean experimental (closed symbols) and model pressure-volume behavior (open symbols) at three different ratios of the material constants b_1/b_2; global stiffness was maintained by decreasing C as b_1 increased. (*b*) Corresponding mean experimental and model shape/volume curves. Increasing fiber stiffness decreases sphericalization during filling. (*c*) Model behavior across a larger range of material constants. The model covers the 95% confidence interval of the experimental normalized shape change ratios ($\Delta S/(\Delta V/\mathrm{ED}V)$, solid circles) with a four-fold variation in b_1/b_2 for a symmetric fiber distribution (open circles). With a 10 deg shift in the fiber distribution a 15-fold change in the b_1/b_2 ratio is required to simulate the same range of shape changes (open triangles).

References

[1] Rankin, J. S., McHale, P. A., Arentzen, C. E., Ling, D., Greenfield, J. C., and Anderson, R. W., 1976, ''The three-dimensional dynamic geometry of the left ventricle in the conscious dog,'' Circ. Res., **39**, 304–313.

[2] Rankin, J. S., 1980, ''The chamber dynamics of the intact left ventricle,'' In: Baan J, Arntzenius AC, Yellin EL, eds. *Cardiac Dynamics*. The Hague, Boston, London: Martinus Nijhoff, 95–106.

[3] Olsen, C. O., Rankin, J. S., Arentzen, C. E., Ring, W. S., HcHale, P. A., and Anderson, R. W., 1981, ''The deformational characteristics of the left ventricle in the conscious dog,'' Circ. Res., **49**, 843–855.

[4] Azancot, A., Caudell, T., Allen, H. D., Toscani, G., Debrux, J. L., Lamberti, A., Sahn, D. J., and Goldberg, S. J., 1985, ''Echocardiographic ventricular shape analysis in congenital heart disease with right ventricular volume or pressure overload,'' Am. J. Cardiol., **56**, 520–526.

[5] Sundblad, P., and Wranne, B., 2002, ''Influence of posture on left ventricular \long and short-axis shortening,'' Am. J. Physiol. Heart Circ. Physiol., **283**, H1302–1306.

[6] Gomez-Doblas, J. J., Schor, J., Vignola, P., Weinberg, D., Traad, E., Carrillo, R., Williams, D., and Lamas, G. A., 2001, ''Left ventricular geometry and operative mortality in patients undergoing mitral valve replacement,'' Clin. Cardiol., **24**, 717–722.

[7] Yettram, A. L., and Beecham, M. C., 1998, ''An analytical method for the determination of along-fibre to cross-fibre elastic modulus ratio in ventricular myocardium—a feasibility study,'' Med. Eng. Phys., **20**, 103–108.

[8] Janz, R. F., Kubert, B. R., Pate, E. F., and Moriarty, T. F., 1980, ''Effect of shape on pressure-volume relationships of ellipsoidal shells,'' Am. J. Physiol. Heart Circ. Physiol., **238**, H917–926.

[9] Demer, L. L., and Yin, F. C. P., 1983, ''Passive biaxial mechanical properties of isolated canine myocardium,'' J. Physiol., **339**, 615–630.

[10] Yin, F. C. P., Strumpf, R. K., Chew, P. H., and Zeger, S. L., 1987, ''Quantification of the mechanical properties of noncontracting canine myocardium under simultaneous biaxial loading,'' J. Biomech., **20**, 577–589.

[11] Humphrey, J. D., Strumpf, R. K., and Yin, F. C. P., 1990, ''Determination of a constitutive relation for passive myocardium: II. parameter estimation,'' J. Biomech. Eng., **112**, 340–346.

[12] Guterl, K. A., and Holmes, J. W., 2002, ''Candidate mechanical stimuli for hypertrophy during early volume overload,'' *Proc. IV World Congress of Biomechanics*, Calgary, Canada.

[13] ILAR, 1996, ''Guide for the care and use of laboratory animals,'' Washington, D.C.: National Academy Press.

[14] Streeter, Jr., D. D., and Hanna, W. T., 1973, ''Engineering mechanics for successive states in canine left ventricular myocardium. I. Cavity and wall geometry,'' Circ. Res., **33**, 639–655.

[15] Costa, K. D., Hunter, P. J., Wayne, J. S., Waldman, L. K., Guccione, J. M., and McCulloch, A. D., 1996, ''A three-dimensional finite element method for large elastic deformations of ventricular myocardium: II—Prolate spheroidal coordinates,'' J. Biomech. Eng., **118**, 464–472.

[16] Emery, J. L., and Omens, J. H., 1997, ''Mechanical regulation of myocardial growth during volume-overload hypertrophy in the rat,'' Am. J. Physiol. Heart Circ. Physiol., **273**, H1198–H1204.

[17] Emery, J. L., Omens, J. H., and McCulloch, A. D., 1997, ''Biaxial mechanics of the passively overstretched left ventricle,'' Am. J. Physiol. Heart Circ. Physiol., **272**, H2299–H2305.

[18] Omens, J. H., MacKenna, D. A., and McCulloch, A. D., 1993, ''Measurement of strain and analysis of stress in resting rat left ventricular myocardium,'' J. Biomech., **26**, 665–676.

[19] Omens, J. H., Milkes, D. E., and Covell, J. W., 1995, ''Effects of pressure overload on the passive mechanics of the rat left ventricle,'' Ann. Biomed. Eng., **23**, 152–163.

[20] Streeter, Jr., D. D., and Hanna, W. T., 1973, ''Engineering mechanics for successive states in canine left ventricular myocardium. II. Fiber angle and sarcomere length,'' Circ. Res., **33**, 656–664.

[21] MacKenna, D. A., Omens, J. H., McCulloch, A. D., and Covell, J. W., 1994, ''Contribution of collagen matrix to passive left ventricular mechanics in isolated rat hearts,'' Am. J. Physiol. Heart Circ. Physiol., **266**, H1007–H1018.

[22] LeGrice, I. J., Smaill, B. H., Chai, L. Z., Edgar, S. G., Gavin, J. B., and Hunter, P. J., 1995, ''Laminar structure of the heart: ventricular myocyte arrangement and connective tissue architecture in the dog,'' Am. J. Physiol. Heart Circ. Physiol. **269**, H571–582.

[23] Legrice, I. J., Hunter, P. J., and Smaill, B. H., 1997, ''Laminar structure of the heart: a mathematical model,'' Am. J. Physiol. Heart Circ. Physiol. **272**, H2466–2476.

[24] Omens, J. H., Farr, D. D., McCulloch, A. D., and Waldman, L. K., 1996, ''Comparison of two techniques for measuring two-dimensional strain in rat left ventricles,'' Am. J. Physiol. Heart Circ. Physiol., **271**, H1256–H1261.

[25] Stevens, C., Remme, E., LeGrice, I., and Hunter, P., 2003, ''Ventricular mechanics in diastole: material parameter sensitivity,'' J. Biomech., **36**, 737–748.

[26] Usyk, T. P., Mazhari, R., and McCulloch, A. D., 2000, ''Effect of laminar orthotropic myofiber architecture on regional stress and strain in the canine left ventricle,'' J. Elast., **61**, 143–164.

[27] Omens, J. H., and Fung, Y.-C., 1990, ''Residual strain in rat left ventricle,'' Circ. Res., **66**, 37–45.